

# Separating and Tracking Multiple Beacon Sources for Deep Space Optical Communications

Kevin M. Birnbaum\*, Adit Sahasrabudhe†, and William H. Farr\*

*We propose a solution for pointing and tracking an optical terminal using one or more beacons and a slowly varying background image. The primary application is a deep space optical communication terminal, where multiple source tracking provides robustness against beacon outage. Our solution uses optical orthogonal codes modulated on each beacon to separate the signal from each source for centroiding. This technique allows calculation of the transmit pointing vector from each beacon location as well as from the background image. The latter can be used to track during beacon outages. We present a simple algorithm for performing this separation, and apply it to experimental data from a photon-counting detector illuminated by two beacons and one constant source. Our results show that the photon flux from each source can be accurately estimated even in the low signal, high background regime.*

## I. Introduction

NASA is developing optical communications for future deep space telecommunications links to provide for increased data volume returns. Aside from operating in a presently unallocated region of the electromagnetic spectrum, the primary advantage of optical communications is a decreased transmitted energy per bit requirement as compared to conventional microwave telecommunications. This is achieved by using transmit beam widths of only a few microrad with antenna apertures of only a few tens of centimeters. For instance, a 1550-nm transmission from a 50-cm diameter antenna has a 3.1-microrad diffraction limited beam width, which would result in a receive footprint on Earth of only 465 km at 1 AU. This can be compared to a 32-GHz (Ka-band) transmit beam width of

---

\*Optical Communications Group

†Advanced Signal Processing Group

The research described in this publication was carried out by the Jet Propulsion Laboratory, California Institute of Technology, under a contract with the National Aeronautics and Space Administration. ©2009 California Institute of Technology. Government sponsorship acknowledged.

3.125 millirad from a 3-m diameter antenna, which would result in a receive footprint of over 468,000 km at 1 AU, or about 73 times the diameter of the Earth.

A major challenge in implementing an optical communications link is pointing such narrow beams. Image centroiding of the illuminated Earth crescent does not provide sufficient pointing knowledge due to sun angle, seasonal and daily land/sea/cloud variations [1]. Present scenarios for deep space operations out to a few AU call for transmission of an optical beacon from Earth to serve as a pointing reference. The Earth beacon is a high power transmission of a broad laser beam, perhaps on the order of 20 to 50 microrad, that can be blind pointed to the spacecraft optical communications terminal. That terminal then measures the angle of arrival in its local coordinate system, and subsequently uses that angle plus a calculated point-ahead correction term for transverse velocity to point the outgoing transmit beam such as to hit a receive station on Earth.

Although beacon transmission from an Earth orbiting platform would be operationally desirable, cost considerations will place initial beacon transmitter stations on Earth's surface. These do not necessarily need to be co-located with receive station locations. However, laser transmissions from Earth's surface to space pass through commercial airspace, necessitating a suite of safety and predictive avoidance systems to prevent hazardous exposure of laser radiation to either people or critical equipment such as Earth orbiting observation satellites. The end result is that laser beacon transmissions can be interrupted for periods of seconds to tens of seconds, resulting in loss of pointing knowledge to the spacecraft optical communications terminal.

In this article, we outline a robust solution for such outages by tracking on multiple sources, and experimentally investigate a method for differentiating those sources using optical orthogonal codes (OOCs) [2, 3]. As multiple beacon stations might not be spatially resolved at the spacecraft optical terminal imager, OOCs are used to distinguish centroids for each beacon and the Earth image. We demonstrate how the signal from a single-photon counting detector (e.g. each pixel in a focal plane array) can be analyzed to determine the optical power from each source.

## II. Utilizing Multiple Sources

In order to generate pointing knowledge, the spacecraft terminal images the sun-illuminated Earth and all active uplink beacons on a detector array. Figure 1 is a diagram of the Earth and the various ground stations as seen from the spacecraft. The point  $E$  represents the centroid of the Earth image, whose position varies slowly with respect to the geometrical center of the Earth due to cloud patterns, sun angle, etc. The points  $A$  and  $B$  represent the locations of the uplink beacon ground stations, and  $R$  represents the downlink receiver station that the spacecraft terminal is targeting.

The centroid of the composite image including all of these sources makes a poor pointing reference, since the relative irradiance of each source is not well known and the Earth image varies. However, each beacon alone can be used to provide improved pointing

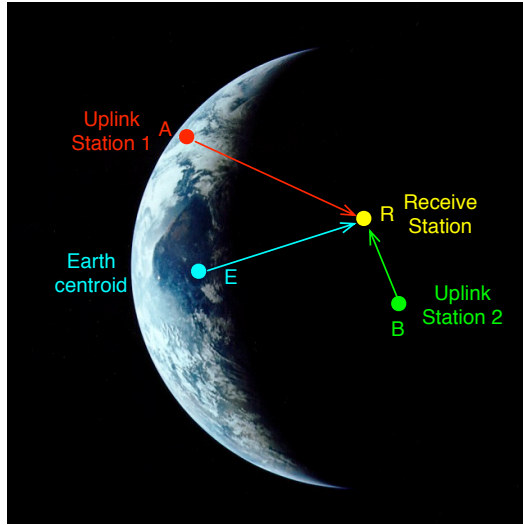


**Figure 1. Diagram of the Earth and ground stations as seen from the spacecraft. The offset vectors from the beacons (uplink stations and Earth centroid) to the ground receiver station are shown.**

accuracy. It is advantageous therefore to separate each of these sources from the overall image. One common way to achieve this is via wavelength division multiplexing, where each source has a different wavelength and narrowband dichroics or optical filters are used on the spacecraft to perform the separation. This approach, however, adds to the cost and complexity of the spacecraft terminal. The simpler alternative solution posed here uses code division multiplexing to determine the amount of light on each pixel coming from each source by modulating the uplink beams and demodulating the received signal.

This modulation can also be used to carry uplink data via various methods. One method would be to convolve the codewords with a generalized on-off keying (e.g. pulse position modulation) signal [4, 5]; another method would assign each uplink station 2 codewords. In the latter case, one codeword would be used to signify the transmission of a 0 bit, while the other would signify a 1. Using either technique, the same array sensor can be used for demodulation as well as acquisition and tracking.

The uplink data may include information about the pointing vector from each uplink station to the receive station (i.e.  $\vec{AR}$  and  $\vec{BR}$  in Figure 1). Alternatively, the orthogonal codeword could be used to identify the uplink station, and the spacecraft could have prior knowledge of the pointing vector from each uplink station to  $R$ . Once the spacecraft has an accurate estimate of the location of  $R$  from one or more uplink beacons, it may also compute the vector  $\vec{ER}$  from the Earth centroid to the receive station. In the event that all uplink stations experience an outage, the spacecraft may then use the Earth centroid and  $\vec{ER}$  to point the downlink beam for several minutes before changes in the Earth image degrade the pointing accuracy. This pointing concept is represented by the state flow diagram in Figure 2.

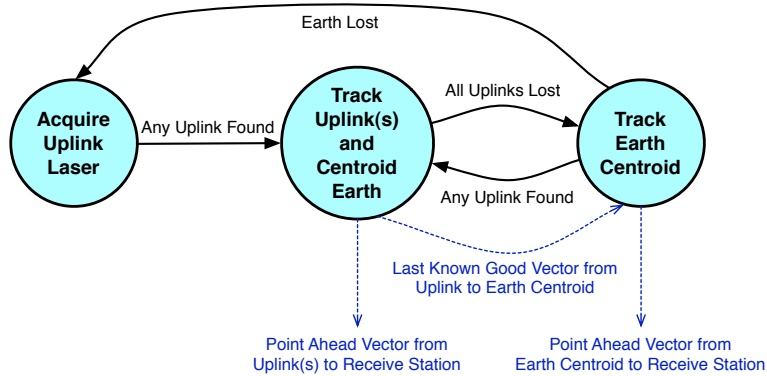


Figure 2. Acquisition, tracking, and pointing operational concept. Solid black arrows indicate state transitions; dashed blue arrows represent input/output information.

### III. Optical Orthogonal Codes

The above scheme is built upon the ability to use the coded uplink modulations to estimate the power from each source at each detector element. We will now discuss how this may be achieved using OOCs.

OOCs are a family of codes with low cross-correlations and autocorrelations which are low at non-zero time offsets. The signal space under consideration is  $\{0, 1\}$ , so the undesirable correlations cannot be made strictly zero at all offsets. However, we can specify the conditions

$$\sum_{k=0}^{n-1} c_k^p c_{k+j}^q \leq 1 \quad \forall j, \forall p \neq q \quad (1)$$

$$\sum_{k=0}^{n-1} c_k^i c_{k+j}^i \leq 1 \quad \forall j \neq 0, \forall i \quad (2)$$

where  $n$  is the number of chips (length) of the binary codewords  $\{\vec{c}^i\}$ . Subscripts are considered modulo  $n$ , that is  $c_k^i = c_{k \bmod n}^i$ , so these are conditions under circular correlations. The weight of the codewords is  $w = \sum_k c_k^i$ . The length required to generate  $\Phi$  codewords with weight  $w$  is bound [2] by

$$n \geq \Phi w(w - 1) + 1 \quad (3)$$

The photon flux (which is proportional to optical power) incident on the detector may be written  $\lambda_T(t) = \lambda_b(t) + \sum_i \lambda_i(t)$ , where  $\lambda_i(t)$  is the photon flux from source  $i$  and  $\lambda_b(t)$  is from the background. As a function of time  $t$ , the fluxes are

$$\lambda_i(t) = \mu_i \sum_{k=-\infty}^{\infty} c_k^i \text{Rect} \left( \frac{t - kT_c^i - b_i}{T_c^i} \right) \quad (4)$$

where  $\mu_i$  is proportional to the peak optical power from source  $i$ ,  $T_c^i$  is the time per chip of codeword  $i$ , and  $b_i$  is the starting time of codeword  $i$ . The rectangular function is defined

by

$$\text{Rect}(u) = \begin{cases} 0 & u < -\frac{1}{2}, u \geq \frac{1}{2} \\ 1 & -\frac{1}{2} \leq u < \frac{1}{2} \end{cases} \quad (5)$$

The background  $\lambda_b(t) = \mu_b$  is constant.

For a photon-counting detector, the incident light will cause electrical pulses at the nondeterministic times  $\{\tau_j\}$ . The generation of electrical pulses is a Poisson process, where the probability of  $\tau$  being within a small range of times  $\Delta t$  is related to  $\lambda_T$  by

$$\lim_{\Delta t \rightarrow 0} \frac{P(t < \tau < t + \Delta t)}{\Delta t} = \lambda_T(t) \quad (6)$$

The electrical pulse associated with each event lasts a time  $\delta$ . The electrical signal is compared to a threshold and sampled at times  $kT_s$  for  $k = \{0, \dots, N-1\}$ . The thresholded sampled signal,  $\vec{x}$ , has value  $\{0, 1\}$  at each of the  $N$  sample times. For low fluxes,

$$K_T = \sum_{k=0}^{N-1} x_k \approx \frac{\delta}{T_s} \int_0^{NT_s} \lambda_T(t) dt \quad (7)$$

where  $K_T$  is the total number of detection events (counts) in the record over a time  $NT_s$ . Similarly,  $K_i, K_b$  are the number of events from source  $i$  and the background, respectively.

We define a normalized frequency  $\alpha_i = T_s/T_c^i$  and a normalized time  $\beta_i = b_i/T_s$ . Then we may define a normalized sampled codeword as

$$y_k^i(\alpha, \beta) = \lambda_i(kT_s)/\mu_i = c_{\text{round}[\alpha(k-\beta)]}^i \quad k \in \{0, \dots, N-1\} \quad (8)$$

Given that the sample clock is not synchronized to the sources, we must find  $\{\alpha_i\}, \{\beta_i\}$  from the measurement record  $\vec{x}$ . We assume a priori knowledge may be used to restrict all  $\{\alpha_i\} \in [\alpha_{min}, \alpha_{max}]$ . Since the signals are periodic, we may restrict the domain of  $\{\beta_i\}$  to  $\beta \in [0, n/\alpha]$  without loss of generality. We find the estimates  $\hat{\alpha}_i, \hat{\beta}_i$  by computing

$$(\hat{\alpha}_i, \hat{\beta}_i) = \arg \max_{\alpha, \beta} R_i(\alpha, \beta) \quad (9)$$

where

$$R_i(\alpha, \beta) = \sum_{k=0}^{N-1} y_k^i(\alpha, \beta) x_k \quad (10)$$

This method of synchronizing to the sources is not optimal, but was chosen for its simplicity and ease of implementation.

Using these estimated parameters, we will attempt to decompose the measurement record to find out how many of the detection events came from each source. We begin by defining an estimated sampled codeword

$$\hat{\vec{y}}_i = \vec{y}_i(\hat{\alpha}_i, \hat{\beta}_i) \quad (11)$$

We then project the data vector  $\vec{x}$  onto the  $(\Phi + 1)$ -dimensional subspace spanned by the set of estimated codewords  $\{\hat{\vec{y}}_i\}$  and the constant word  $\vec{y}_b = 1$ . This vector projection in the  $N$ -dimensional space of the measurement record is equivalent to a linear least squares

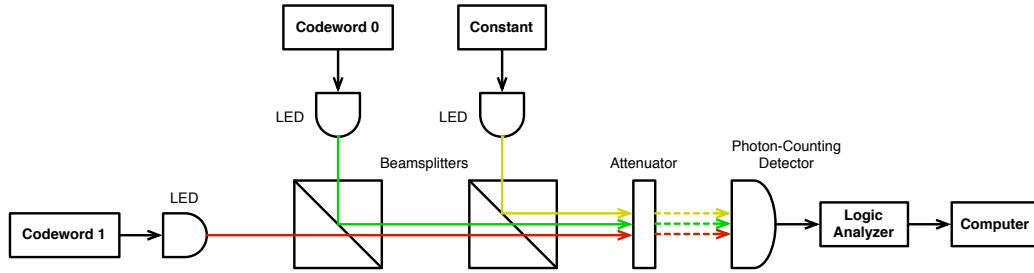


**Figure 3. Multiple beacon test setup.** The codeword 0, codeword 1, and background light sources were added together using beamsplitters, attenuated, and used to illuminate the photon counting detector. The output of the detector was sampled and stored for processing.

fit to the data. The components of the projection along each dimension (codeword) are given by

$$\vec{g} = (A^T A)^{-1} A^T \vec{x} \quad (12)$$

where the dimension of  $\vec{g}$  is  $\Phi + 1$  and

$$A = \begin{bmatrix} \hat{y}_0 & \hat{y}_1 & \cdots & \hat{y}_{\Phi-1} & \vec{y}_b \end{bmatrix} \quad (13)$$

We can therefore estimate that  $\hat{K}_i$  detection events in the record came from source  $i$  where

$$\hat{K}_i = g_i \sum_{k=0}^{N-1} y_k^i \quad i \in \{0, \dots, \Phi - 1\} \quad (14)$$

and  $\hat{K}_b$  events came from the background, where

$$\hat{K}_b = g_\Phi \sum_{k=0}^{N-1} y_b = g_\Phi N \quad (15)$$

#### IV. Experiment

We have tested experimentally the above algorithm for estimating the number of detection events from each source. Conditions were chosen to emulate the photon-starved, low signal-to-noise ratio regime expected for a deep space terminal. Results are presented for a single-element detector, but would be representative of each pixel in a spacecraft terminal's focal plane array.

We tested our algorithm using a photon-counting detector, since they will ultimately be preferred over linear detectors for deep space (photon-starved) applications. The detector we used was an RCA model SPCM-100-PQ [6]. It is a passively quenched detector with an active area of about  $200 \mu\text{m}$  and a peak quantum efficiency listed at  $\approx 43\%$  at 643 nm. Using this detector along with three light sources ( $\Phi = 2$  signal sources and 1 background source), our test setup followed Figure 3. Each signal source is a light emitting diode (LED) driven by an arbitrary waveform generator programmed with the respective

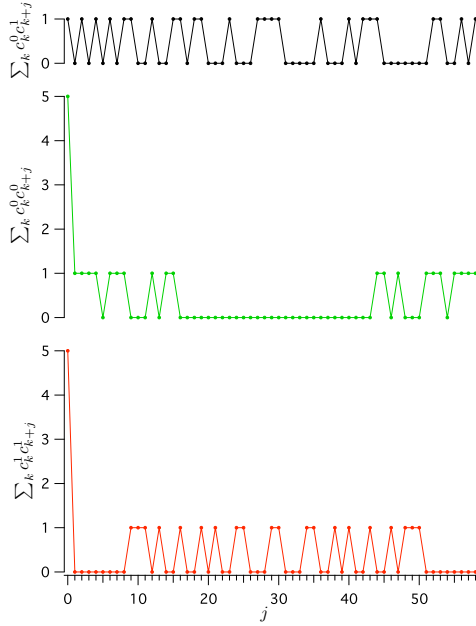


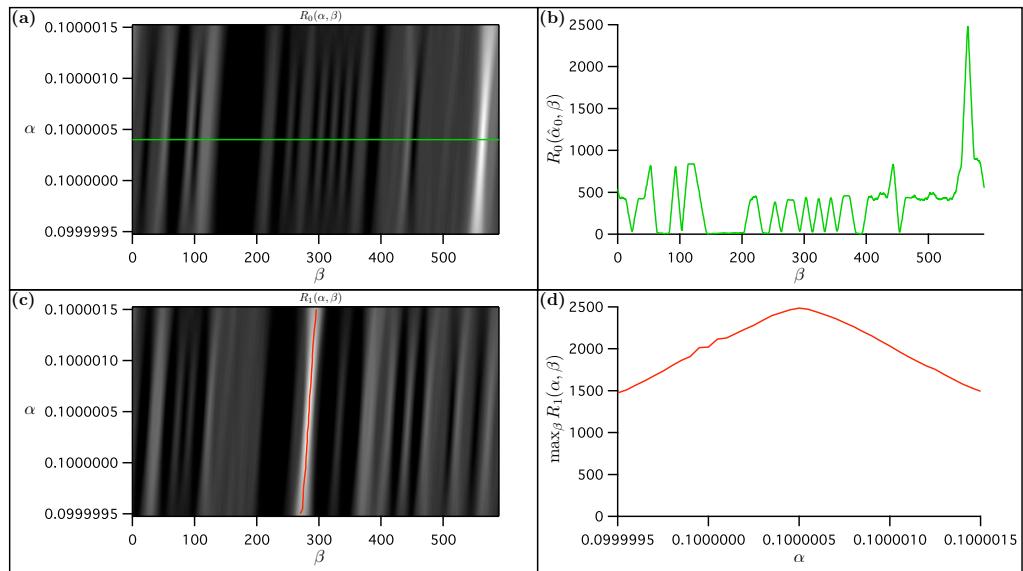
**Figure 4. Correlation properties of codes used in the experiment.**

codeword. The time per chip for codeword 1 was  $T_c^1 = 1 \mu s$  and for codeword 0 was  $T_c^0 = 1.000001 \mu s$ . The difference in these frequencies was chosen to emulate unsynchronized clocks at different ground stations. The background source is an LED driven with a constant current. The detector output was sampled using a 1 bit analog to digital converter (ADC) with one sample per  $T_s = 100$  ns in order to match the approximately  $\delta = 100$  ns pulses from the detector. The record length was  $N = 2 \times 10^6$  samples for each test condition. The clocks on the codeword generators were synchronized to each other but not to the ADC. The codewords had length  $n = 59$  and weight  $w = 5$ . The non-zero entries of codeword 0 are  $\{0, 1, 3, 7, 15\}$  and the non-zero entries of codeword 1 are  $\{0, 9, 19, 30, 43\}$ . The auto- and cross-correlations of these codewords are shown in Figure 4.

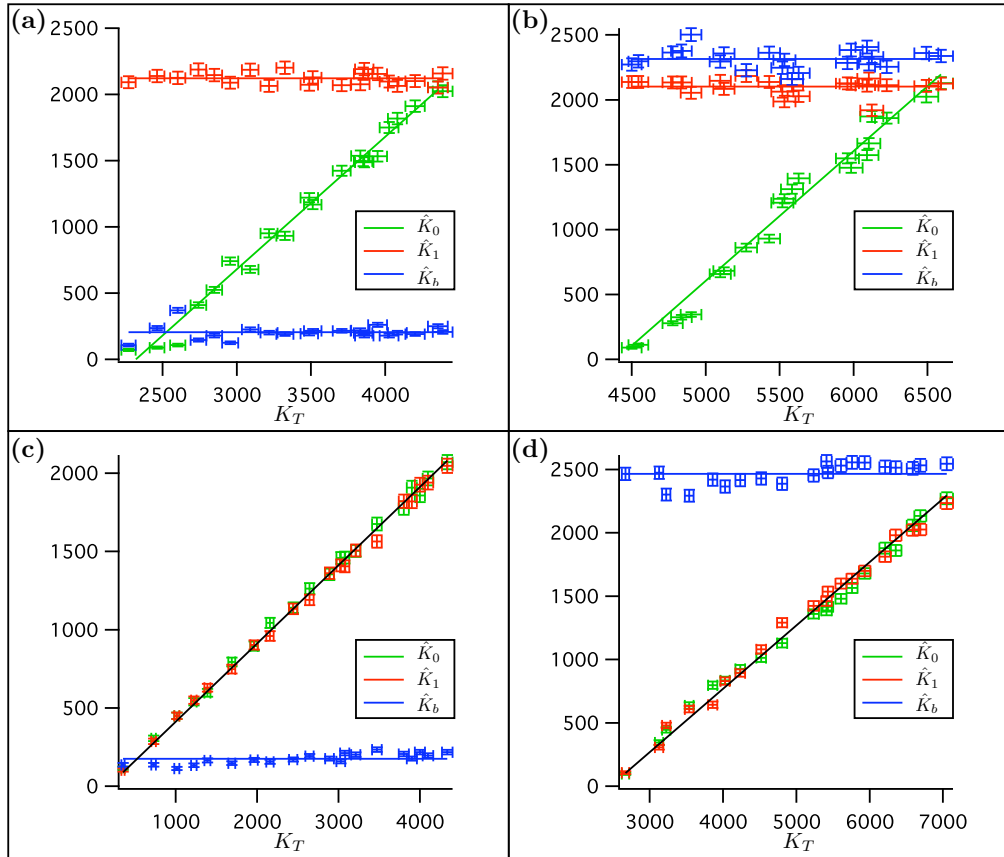
In generating our estimates  $\{\hat{K}_0, \hat{K}_1, \hat{K}_b\}$ , we used  $\alpha_{min} = 0.1$ ,  $\alpha_{max} = 0.100001$  chips/sample. We performed the maximization Eq. 9 over 21 evenly spaced values of  $\alpha$  and 2360 values of  $\beta$ . Examples of the correlations  $R_0(\alpha, \beta), R_1(\alpha, \beta)$  are shown in Figure 5.

Figure 6 shows the estimates  $\{\hat{K}_0, \hat{K}_1, \hat{K}_b\}$  vs. the total count rate  $K_T$  as the power of one or both of the modulated light sources was varied. Figures 6 (a)-(b) demonstrate, as expected, that varying the power from source  $i$  causes variation in the estimate of the corresponding codeword  $\hat{K}_i$  which follows  $\Delta \hat{K}_i = \Delta K_T$ . Similarly, Figures 6 (c)-(d) show that varying two sources  $i$  and  $j$  such that  $\mu_i = \mu_j$  causes their estimates  $\hat{K}_i, \hat{K}_j$  to follow  $\Delta \hat{K}_i = \Delta \hat{K}_j = \Delta K_T/2$ .

In Figure 6(a) we can see that for low optical power in codeword 0, the estimator does not synchronize. As a result, most of the flux from codeword 0 is attributed to the



**Figure 5. Synchronization of a sample measurement record.** For this data set, each of the signal sources was set to give an equal count rate at the detector, and the background rate was set to be much lower. The total number of detection events in the record was  $K_T = 4355$ . (a) The correlation  $R_0(\alpha, \beta)$  is computed for various values of  $\alpha, \beta$  and displayed as a grayscale with black indicating the minimum value and white the maximum value. The green line indicates the estimate  $\hat{\alpha}_0$ . (b) A portion of (a) with fixed  $\alpha = \hat{\alpha}_0$  but variable  $\beta$ . (c) The correlation  $R_1(\alpha, \beta)$  is computed for various values of  $\alpha, \beta$  and displayed as a grayscale with black indicating the minimum value and white the maximum value. The red line indicates the value of  $\beta$  that maximizes  $R_1(\alpha, \beta)$  at each  $\alpha$ . (d) The correlation  $R_1(\alpha, \beta)$  taken along the red line of (c).



**Figure 6.** Estimated number of counts from each source vs. total number of counts. All error bars are equal to the square-root of the plotted value. (a) The optical power of the codeword 0 source was varied while holding the power of the other signal and the background constant. (b) Similar to (a), but with the background source set to a higher optical power. (c) The optical power of the two signal sources were set to each give the same count rate at the detector. That count rate was varied while holding the background source fixed. (d) Similar to (c), but with the background source set to a higher optical power.

background. However, at higher powers both estimators synchronize correctly and the estimates follow the expected trends. We believe that another synchronization algorithm could yield better performance at low photon fluxes.

In conclusion, we have demonstrated that optical orthogonal codes can be used to disambiguate multiple sources with just one detector. This technique was shown to be effective in the photon-counting regime, in the presence of a strong background light, which is the relevant domain for deep space optical communications. This scheme should enable easy handover between multiple beacon sources used for pointing a spacecraft terminal.

### Acknowledgments

Thanks to Bruce Moision for helpful discussions of orthogonal coding.

### References

- [1] C.-C. Chen, "Effect of Earth Albedo Variation on the Performance of a Spatial Acquisition Subsystem Aboard a Planetary Spacecraft," *The Telecommunications and Data Acquisition Progress Report*, vol. 42-95, Jet Propulsion Laboratory, California Institute of Technology, Pasadena, California, pp. 202-211, July-September 1988. [http://ipnpr/progress\\_report/42-95/95T.PDF](http://ipnpr/progress_report/42-95/95T.PDF)
- [2] F. Chung, J. Salehi, and V. Wei, "Optical Orthogonal Codes: Design, Analysis and Applications," *IEEE Transactions on Information Theory*, vol. 35, pp. 595–604, May 1989.
- [3] R. Fuji-Hara and Y. Miao, "Optical Orthogonal Codes: Their Bounds and New Optimal Constructions," *IEEE Transactions on Information Theory*, vol. 46, pp. 2396–2406, November 2000.
- [4] P. Prucnal, M. Santoro, and T. Fan, "Spread Spectrum Fiber-Optic Local Area Network Using Optical Processing," *Journal of Lightwave Technology*, vol. 4, pp. 547–554, May 1986.
- [5] F. Khansefid, R. Gagliardi, and H. Taylor, "Performance Analysis of Code Division Multiple Access Techniques in Fiber Optics with On-Off and PPM Pulsed Signaling," in *Military Communications Conference, 1990. MILCOM '90, Conference Record, A New Era. 1990 IEEE*, pp. 909–915 vol.3, September-October 1990.
- [6] GE Electro Optics, *SPCM-11-PQ Single Photon Counting Module Datasheet*, 1989.